IL NUOVO CIMENTO **47 C** (2024) 15
DOI 10.1393/ncc/i2024-24015-2

Colloquia: COMEX7

γ decay of giant resonances to low-lying states

Y. F. Niu([1]), W. L. Lv ([1]) and G. Colò ([2])

([1]) *School of Nuclear Science and Technology, Lanzhou University and Frontiers Science Center for Rare isotope, Lanzhou University - Lanzhou 730000, China*

([2]) *Dipartimento di Fisica, Università degli Studi di Milano and INFN, Sezione di Milano via Celoria 16, 20133 Milano, Italy*

received 31 October 2023

Summary. — With growing studies on giant resonances, the deep insight about their damping mechanisms draws more and more attentions. Here we provide an alternative way to study the detailed structures of giant resonances apart from the wavelet analysis of the high-resolution strength distribution, including isospin properties and wavefunctions, the latter of which indicates the main damping mechanism of giant resonances. We utilize a fully self-consistent random phase approximation (RPA) + particle vibration coupling (PVC) model to calculate the γ decay width based on Skyrme density functional. We find that the complex configuration, *i.e.*, one-particle one-hole coupled with phonon, has much larger component in the wavefunction of GQR than that of GDR, which indicates the main damping mechanisms in these two modes are different.

1. – Introduction

γ photon is an important and clean probe for nuclear structure. On one hand, it can excite the collective motions of the nucleus, among which the dipole excitation dominates. On the other hand, the decay through emitting γ photon could provide detailed structure information of the corresponding excited state, like the isospin properties and wavefunctions [1,2]. Due to the well-known electromagnetic force, the corresponding cross section or decay width between photon and nucleus are simply related with the transition probabilities. Therefore, photons provide us a very clean probe for seeing the inside of nuclei without complicated reaction mechanism involved. For experimental purpose, it calls for the construction of γ beam facilities. One effective way to generate γ beam is the inverse Compton scattering [3]. The low-energy photons collide with the high-energy electrons, and hence photons obtain energies from electrons to become γ photons. Such facilities include the High Intensity γ-ray Source (HIγS) at Triangle Universities Nuclear Laboratory (TUNL) and the Duke Free Electron Laser Laboratory (DFELL) [4], Extreme Light Infrastructure - Nuclear Physics (ELI-NP) [5], and Shanghai Laser Electron Gamma Source (SLEGS) [6]. The study of giant dipole resonances (GDRs) is one of the important physics goals at such facilities. For example, the microscopic structure and damping mechanism of GDR need further investigation.

In fact, the typical values of the centroid energy of giant resonances are $10-15$ MeV, and the width of the giant resonances are around $3-5$ MeV. It means that the giant vibrations go only through few periods of oscillation before they relax. The resonance width is composed of three parts, which are Landau width, escape width $\Gamma^{\uparrow}$ and spreading width $\Gamma^{\downarrow}$ [7-9]. The Landau width is formed due to the configuration splitting in one-particle-one-hole (1p-1h) configuration space. The escape width is caused by the direct decay of emitting neutrons, protons, alpha particles or γ photons. The spreading width is formed due to the fact that the correlated 1p-1h giant resonance state relaxes into more complex $2p-2h$, $3p-3h$, etc. states, eventually dissolving into the compound nucleus. Although this picture is widely accepted, the direct experimental evidences are not many. The determination of $\Gamma^{\uparrow}$ is possible in experiment, however, what are the relative contributions of Landau width and spreading width? Up to now, this question has only been answered by wavelet analysis of the fine structure of giant resonances. Through the high resolution (p,p') experiments, the fine structure in the energy region of the isoscalar giant quadrupole resonance in nuclei is observed [10]. Based on the wavelet analysis technique, a comparison with microscopic model calculations including 2p-2h degrees of freedom identifies the coupling to surface vibrations as the main source of the observed scales [10]. In contrast, the inclusion of complex configurations in the calculations changes the giant dipole strength distributions but the impact on the wavelet power spectra and characteristic scales is limited, indicating Landau damping as a dominant mechanism responsible for the fine structure of the isovector GDR [11].

However, are there alternative ways to demonstrate the different damping mechanisms in isovector GDR and isoscalar GQR? Direct γ decay of these giant resonances to low-lying states offers a new possibility. Although it is only a tiny part in the escaping width, in this contribution we will show how the γ-decay width provides the isospin properties as well as the details of wavefunctions of giant resonances, which indicates the main damping mechanism. The method we use is the fully self-consistent random phase approximation (RPA) + particle vibration coupling (PVC) approach based on Skyrme density functionals, which was first used for the calculation of γ decay in ref. [12].

In sect. 2, we describe the RPA+PVC formalism for γ-decay calculation. In sect. 3, we provide our main results and discussions. Conclusions and perspectives are drawn in sect. 4. The main conclusion of this paper has been published in ref. [13], however, in this contribution we utilized a different Skyrme interaction to demonstrate the universality of our conclusion, which doesn't depend on the specific Skyrme interactions although the absolute values of γ-decay width are different.

2. – Formalism

The γ-decay width Γ_γ of electronic multipole transition $E\lambda$ is calculated as [14]

$$\Gamma_\gamma(E\lambda; i\to f) = \frac{8\pi(\lambda+1)}{\lambda\left[(2\lambda+1)!!\right]}\left(\frac{E}{\hbar c}\right)^{2\lambda+1} B(E\lambda; i\to f), \tag{1}$$

where E represents the transition energy, and λ is the electronic multipolarity. The reduced transition probability B between the two excited states $|n_i J_i\rangle$ and $|n_f J_f\rangle$ is

$$B(E\lambda; i\to f) = \frac{1}{2J_i+1}\left|\langle n_f J_f||Q^\lambda||n_i J_i\rangle\right|^2, \tag{2}$$

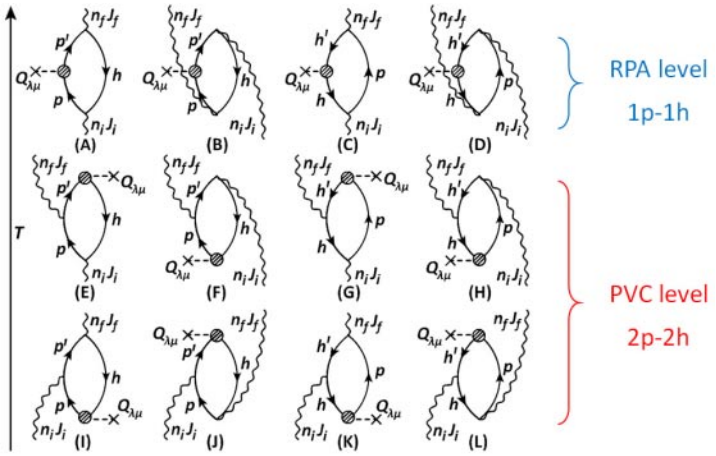

Fig. 1. – The 12 lowest order NFT diagrams in the process of γ-decay between two vibrational states. The circle with lines includes the contribution to $Q_{\lambda\mu}$ from nuclear polarization [12]. The arrow of time is upward.

where Q^λ is the electric multipole operator,

$$
\begin{aligned}
Q^{\lambda\mu} =& \frac{e}{2}\sum_{i=1}^{A}\Big\{\Big[\Big(1-\frac{1}{A}\Big)^{\lambda}+(-)^{\lambda}\frac{2Z-1}{A^{\lambda}}\Big] \\
&-\Big[\Big(1-\frac{1}{A}\Big)^{\lambda}+\frac{(-)^{\lambda+1}}{A^{\lambda}}\Big]\tau_z(i)\Big\} r_i^{\lambda} \mathrm{i}^{\lambda} Y_{\lambda\mu}(\hat{\boldsymbol{r}}_i) \\
\equiv& \frac{1}{2}\sum_{i=1}^{A} e_i^{\mathrm{eff}} r_i^{\lambda} i^{\lambda} Y_{\lambda\mu}(\hat{\boldsymbol{r}}_i).
\end{aligned} \tag{3}
$$

Due to the recoil of the nucleus, the effective charge e_i^{eff} can be induced [14].

The transitions between nuclear ground state and excited states, especially giant resonances(GRs), can be well described by the RPA model [15]. However, for the transitions between two vibrational states, the interplay between single-particle motion and collective vibration will be non-negligible. Therefore, to study the γ decay from GRs to low-lying states, we have to calculate the matrix element $\langle n_f J_f||Q^\lambda||n_i J_i\rangle$ with a beyond RPA model, *i.e.*, RPA+PVC model in present work.

In the RPA+PVC model, we expand the matrix element $\langle n_f J_f||Q^\lambda||n_i J_i\rangle$ to the lowest order, as depicted by the 12 nuclear field theory (NFT) [16,17] diagrams in fig. 1. For all the diagrams, there are two residual interaction vertices. However, diagrams A-D have been naturally included in the RPA model. Diagrams E-L can only appear in the RPA+PVC model because of the PVC vertices, *e.g.*, $\langle p', nJ|V_{\mathrm{res.}}|p\rangle$ in diagram E. Diagrams E, F, G, and H will contribute when the initial phonon has more complex configurations made up with 1p-1h coupled with the final phonon, while diagrams I, J, K, and L will contribute when the final phonon has more complex configurations made up with 1p-1h coupled with the initial phonon. The expressions of these diagrams are given as follows.

$$\langle n_f J_f||Q_\lambda||n_i J_i\rangle_{\rm A} = \sum_{pp'h} \left\{ \begin{array}{ccc} J_i & \lambda & J_f \\ j_{p'} & j_h & j_p \end{array} \right\} \frac{(-)^{J_i+J_f+\lambda+1}\langle p||V_{\rm res.}||h,n_i J_i\rangle\langle h,n_f J_f||V_{\rm res.}||p'\rangle Q^{\lambda{\rm pol}}_{p'p}}{(E_{J_i}-\varepsilon_{ph}+i\eta)(E_{J_f}-\varepsilon_{p'h})}, \tag{4}$$

$$\langle n_f J_f||Q_\lambda||n_i J_i\rangle_{\rm B} = \sum_{pp'h} \left\{ \begin{array}{ccc} J_i & \lambda & J_f \\ j_{p'} & j_h & j_p \end{array} \right\} \frac{(-)\langle h||V_{\rm res.}||p,n_i J_i\rangle\langle p',n_f J_f||V_{\rm res.}||h\rangle Q^{\lambda{\rm pol}}_{pp'}}{(E_{J_i}+\varepsilon_{ph}+i\eta)(E_{J_f}+\varepsilon_{p'h})}, \tag{5}$$

$$\langle n_f J_f||Q_\lambda||n_i J_i\rangle_{\rm C} = \sum_{phh'} \left\{ \begin{array}{ccc} J_i & \lambda & J_f \\ j_{h'} & j_p & j_h \end{array} \right\} \frac{\langle p||V_{\rm res.}||h,n_i J_i\rangle\langle h',n_f J_f||V_{\rm res.}||p\rangle Q^{\lambda{\rm pol}}_{hh'}}{(E_{J_i}-\varepsilon_{ph}+i\eta)(E_{J_f}-\varepsilon_{ph'})}, \tag{6}$$

$$\langle n_f J_f||Q_\lambda||n_i J_i\rangle_{\rm D} = \sum_{phh'} \left\{ \begin{array}{ccc} J_i & \lambda & J_f \\ j_{h'} & j_p & j_h \end{array} \right\} \frac{(-)^{\lambda+J_i+J_f}\langle h||V_{\rm res.}||p,n_i J_i\rangle\langle p,n_f J_f||V_{\rm res.}||h'\rangle Q^{\lambda{\rm pol}}_{h'h}}{(E_{J_i}+\varepsilon_{ph}+i\eta)(E_{J_f}+\varepsilon_{ph'})}, \tag{7}$$

$$\langle n_f J_f||Q_\lambda||n_i J_i\rangle_{\rm E} = \sum_{pp'h} \left\{ \begin{array}{ccc} J_i & \lambda & J_f \\ j_{p'} & j_p & j_h \end{array} \right\} \frac{(-)\langle p||V_{\rm res.}||h,n_i J_i\rangle\langle p',n_f J_f||V_{\rm res.}||p\rangle Q^{\lambda{\rm pol}}_{hp'}}{(E_{J_i}-\varepsilon_{ph}+i\eta)(E_{J_i}-E_{J_f}-\varepsilon_{p'h}+i\eta')}, \tag{8}$$

$$\langle n_f J_f||Q_\lambda||n_i J_i\rangle_{\rm F} = \sum_{pp'h} \left\{ \begin{array}{ccc} J_i & \lambda & J_f \\ j_{p'} & j_p & j_h \end{array} \right\} \frac{(-)^{\lambda+J_i+J_f+1}\langle h||V_{\rm res.}||p,n_i J_i\rangle\langle p,n_f J_f||V_{\rm res.}||p'\rangle Q^{\lambda{\rm pol}}_{p'h}}{(E_{J_i}+\varepsilon_{ph}-i\eta)(E_{J_i}-E_{J_f}+\varepsilon_{p'h}-i\eta')}, \tag{9}$$

$$\langle n_f J_f||Q_\lambda||n_i J_i\rangle_{\rm G} = \sum_{phh'} \left\{ \begin{array}{ccc} J_i & \lambda & J_f \\ j_{h'} & j_h & j_p \end{array} \right\} \frac{(-)^{\lambda+J_i+J_f}\langle p||V_{\rm res.}||h,n_i J_i\rangle\langle h,n_f J_f||V_{\rm res.}||h'\rangle Q^{\lambda{\rm pol}}_{h'p}}{(E_{J_i}-\varepsilon_{ph}+i\eta)(E_{J_i}-E_{J_f}-\varepsilon_{ph'}+i\eta')}, \tag{10}$$

$$\langle n_f J_f||Q_\lambda||n_i J_i\rangle_{\rm H} = \sum_{phh'} \left\{ \begin{array}{ccc} J_i & \lambda & J_f \\ j_{h'} & j_h & j_p \end{array} \right\} \frac{\langle h||V_{\rm res.}||p,n_i J_i\rangle\langle h',n_f J_f||V_{\rm res.}||h\rangle Q^{\lambda{\rm pol}}_{ph'}}{(E_{J_i}+\varepsilon_{ph}-i\eta)(E_{J_i}-E_{J_f}+\varepsilon_{ph'}-i\eta')}, \tag{11}$$

(12)
$$\langle n_f J_f||Q_\lambda||n_i J_i\rangle_{\rm I} = \sum_{pp'h} \left\{ \begin{array}{ccc} J_i & \lambda & J_f \\ j_h & j_{p'} & j_p \end{array} \right\} \frac{\langle p'||V_{\rm res.}||p, n_i J_i\rangle\langle h, n_f J_f||V_{\rm res.}||p'\rangle Q^{\lambda{\rm pol}}_{ph}}{(E_{J_f} - \varepsilon_{p'h})(E_{J_i} - E_{J_f} + \varepsilon_{ph} + i\eta)},$$

(13)
$$\langle n_f J_f||Q_\lambda||n_i J_i\rangle_{\rm J} = \sum_{pp'h} \left\{ \begin{array}{ccc} J & \lambda & J_f \\ j_h & j_{p'} & j_p \end{array} \right\} \frac{(-)^{\lambda+J_i+J_f}\langle p||V_{\rm res.}||p', n_i J_i\rangle\langle p', n_f J_f||V_{\rm res.}||h\rangle Q^{\lambda{\rm pol}}_{hp}}{(E_{J_i} - E_{J_f} - \varepsilon_{ph} + i\eta)(E_{J_f} + \varepsilon_{p'h})},$$

(14)
$$\langle n_f J_f||Q_\lambda||n_i J_i\rangle_{\rm K} = \sum_{phh'} \left\{ \begin{array}{ccc} J_i & \lambda & J_f \\ j_p & j_{h'} & j_h \end{array} \right\} \frac{(-)^{\lambda+J_i+J_f+1}\langle h||V_{\rm res.}||h', n_i J_i\rangle\langle h', n_f J_f||V_{\rm res.}||p\rangle Q^{\lambda{\rm pol}}_{ph}}{(E_{J_i} - E_{J_f} + \varepsilon_{ph} + i\eta)(E_{J_f} - \varepsilon_{ph'})},$$

(15)
$$\langle n_f J_f||Q_\lambda||n_i J_i\rangle_{\rm L} = \sum_{phh'} \left\{ \begin{array}{ccc} J_i & \lambda & J_f \\ j_p & j_{h'} & j_h \end{array} \right\} \frac{(-)\langle h'||V_{\rm res.}||h, n_i J_i\rangle\langle p, n_f J_f||V_{\rm res.}||h'\rangle Q^{\lambda{\rm pol}}_{hp}}{(E_{J_i} - E_{J_f} - \varepsilon_{ph} + i\eta')(E_{J_f} + \varepsilon_{ph'})}.$$

The initial and final vibrational states $|n_i J_i\rangle$ and $|n_f J_f\rangle$, denoted by a wavy line in fig. 1, are calculated with the fully self-consistent RPA method [18]. We include the nuclear polarization effect in operator $Q^{\lambda{\rm pol}}$ [17], which reads

(16)
$$Q^{\lambda{\rm pol}}_{kl} \equiv \langle k||Q^\lambda||l\rangle + \langle k||Q^{\lambda{\rm corr}}||l\rangle,$$

where k and l can be either particle or hole state, and the correction part is
(17)
$$\langle k||Q^{\lambda{\rm corr}}||l\rangle = \sum_{n'} \frac{1}{\sqrt{2\lambda+1}} \Big[\frac{\langle 0||Q^\lambda||n'\lambda\rangle\langle k, n'\lambda||V||l\rangle}{E_{J_i} - E_{J_f} - E_\lambda + {\rm i}\eta} - \frac{\langle k||V||l, n'\lambda\rangle\langle n'\lambda||Q^\lambda||0\rangle}{E_{J_i} - E_{J_f} + E_\lambda + {\rm i}\eta} \Big].$$

3. – Results and discussions

The imaginary part η and η' are set as 0.5 MeV to take into account the coupling to more complicated configurations. More numerical details can be found in ref. [13]. It is worth noting that we use a large configuration space with the single-particle energy cut-off $\varepsilon_{\rm cut} = 150$ MeV. As an example, the Skyrme functional LNS [19] is used, because the properties of low-lying states and GRs in ^{208}Pb can be reasonably described. By checking the results of other Skyrme functionals, we find our main conclusions are independent from the choice of effective interaction.

We first study the isospin property of GRs from their γ decay. We compare the total γ-decay widths $\Gamma^{\rm tot}_\gamma$, the contribution from proton Γ^π_γ, and the contribution from neutron Γ^π_γ. Results are plotted in fig. 2(a). The total γ-decay width $\Gamma^{\rm tot}_\gamma$ of the GDR $\to 2^+_1$ is 285.74 eV, which is more than twice than that of the GQR $\to 3^-_1$, 123.54 eV. However, the contributions from proton or neutron are quite different in these two cases. The Γ^π_γ

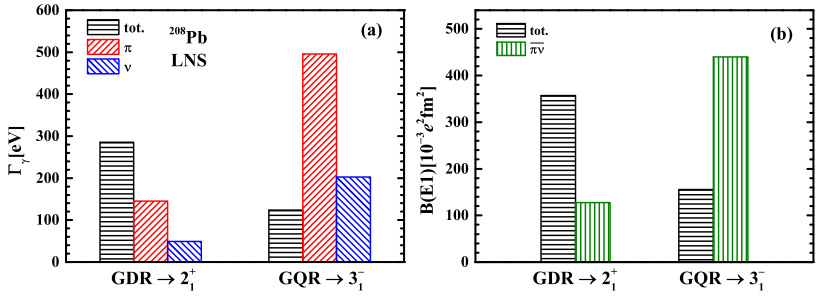

Fig. 2. – Comparison of the γ-decay widths between GDR $\to 2_1^+$ and GQR $\to 3_1^-$ in ^{208}Pb (panel (a)). The total γ-decay widths (tot.) are shown, as well as the contributions from protons (π) and neutrons (ν). Comparison of the transition probabilities $B(E1)$ between GDR $\to 2_1^+$ and GQR $\to 3_1^-$ in ^{208}Pb (panel (b)). Here, the total $B(E1)$ and the average of contributions from protons and neutrons $B^{\overline{\pi\nu}}(E1)$ are displayed.

and Γ_γ^ν in the GDR $\to 2_1^+$ are both much smaller that the $\Gamma_\gamma^{\rm tot}$, while it is inverse in the γ decay of GQR $\to 3_1^-$. This phenomena results from the different isospin character of GDR and GQR [1, 20]. The low-lying states 2_1^+ and 3_1^- are isoscalar, which can be inferred from the same phase of the transition densities of proton and neutron (see fig. 3(a) and (b)). From fig. 3(c) and (d), we can also learn that the GDR is isovector while the GQR is isoscalar. Then under the isovector operator of $E1$, the relative phase of protons and neutrons in GRs will be changed, so that we finally observe the coherent contributions of protons and neutrons in GDR $\to 2_1^+$, while the incoherent contributions of protons and neutrons in GQR $\to 3_1^-$. Such conclusion can be further proven in the limit of exact isospin symmetry in $N = Z$ nucleus ^{56}Ni [13].

On the other hand, we notice that the Γ_γ^π and Γ_γ^ν in the decay of GDR are, respectively, 145.11 eV and 49.15 eV, while in the decay of GQR they are both 3-4 times larger, namely 495.63 eV and 202.42 eV. Since the transition energy is one of the factors involved in the expression of decay widths, we directly compare the total transition probability $B(E1)$ as well as the values of $B^{\overline{\pi\nu}}(E1)$ in fig. 2(b). Here we use $B^{\overline{\pi\nu}}(E1)$ to represent the average contributions of protons and neutrons, which excludes the isospin effects. Similar as the

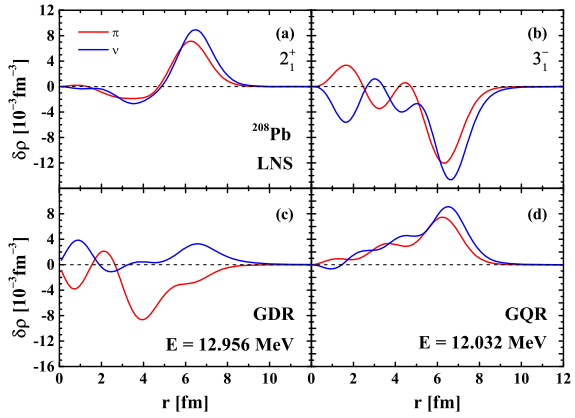

Fig. 3. – The transition densities of the low-lying states (panels (a) and (b)) and GRs (panels (c) and (d)) For the GRs, only the most prominent states are shown.

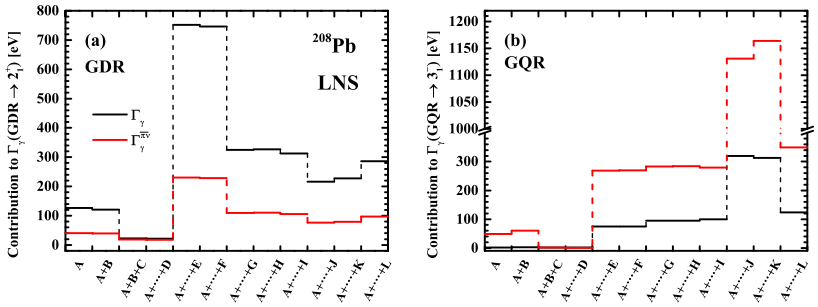

Fig. 4. – The cumulative γ-decay widths Γ_γ of 12 NFT diagrams of (a) GDR$\rightarrow 2_1^+$ and (b) GQR$\rightarrow 3_1^-$ in ^{208}Pb. The black line is the total decay width, while the red line is the average value of the contribution from proton and neutron.

results of γ decay widths, $B(E1)$ for the GDR decay is about 2 times larger than that for the GQR decay, while $B^{\overline{\pi\nu}}(E1)$ for the GDR decay is less than $\frac{1}{2}$ of the value for GQR decay. The relation about $B^{\overline{\pi\nu}}(E1)$ is related to the wave functions of the initial state $|n_i J_i\rangle$ and final $|n_f J_f\rangle$, which will be carefully studied later.

As stated before, the component of low-lying phonons in the wave functions of the GRs can be learned by analyzing the contribution of different NFT diagrams. Therefore, we compare the contributions of each diagram to the γ-decay widths, as depicted in fig. 4. For the Γ_γ of GDR $\rightarrow 2_1^+$, the contributions from diagrams in RPA level almost cancel each other, particularly for diagrams A and C. The decay width in this case is mainly contributed by the diagrams at PVC level, which clearly shows the importance of the PVC effect when studying the γ decay in two vibrational states. Diagrams E and G are the two essential diagrams, which yield 76% of the total width. The case in Γ_γ of GQR $\rightarrow 3_1^-$ is very similar. Although the individual contributions from diagram J and K are remarkable, they cancel each other to a very large extent. Therefore, diagrams E and G yield 95% of the total width in this case. Such a small contribution from diagrams I, J, K and L is understandable, because only when the coupling of 1p-1h configurations with the GR, $|[(ph)_J \otimes J_i]_{J_f}\rangle$, in the wave functions of low-lying state is large, the contribution from diagrams I, J, K and L could be enhanced.

Diagrams E and G dominate the γ-decay width and they represent the contributions (at PVC level) that arise when the wave function of the initial phonon has the component $|[(ph)_J \otimes J_f]_{J_i}\rangle$, which makes it possible to learn the wave functions of GDR and GQR from their γ decay. Because $B^{\overline{\pi\nu}}(E1;\mathrm{GDR} \rightarrow 2_1^+) < 0.5B^{\overline{\pi\nu}}(E1;\mathrm{GQR} \rightarrow 3_1^-)$, the $|[(ph)_J \otimes 3_1^-]_{\mathrm{GQR}}\rangle$ component in the wave function of the GQR is much larger than the $|[(ph)_J \otimes 2_1^+]_{\mathrm{GDR}}\rangle$ component in the wave function of the GDR. This conclusion is in agreement with that of the wavelet analysis [10, 11].

4. – Conclusions

In summary, the γ decay from GRs to low-lying states in ^{208}Pb are studied with the RPA+PVC model by calculating the lowest order NFT diagrams. The isospin-enhancing and suppressing effects are respectively observed in the results of Γ_γ of GDR $\rightarrow 2_1^+$ and GQR $\rightarrow 3_1^-$ in ^{208}Pb. To avoid the influence of isospin properties of the GDR and GQR of ^{208}Pb, we directly compare $B^{\overline{\pi\nu}}(E1)$, the average value of $B^{\pi}(E1)$ and $B^{\nu}(E1)$. It

is found that $B^{\overline{\pi\nu}}(E1)$ of GQR $\rightarrow 3^-_1$ is much larger than the value of GDR $\rightarrow 2^+_1$. Combining with the fact that the contribution to Γ_γ is dominated by the configuration of $1p$-$1h$ coupling to a low-lying phonon, *i.e.*, diagram E and G, we conclude that the $|(ph)_J \otimes 3^-_1\rangle$ component in the wave function of the GQR is larger than the $|(ph)_J \otimes 2^+_1\rangle$ component in the wave function of the GDR.

This work demonstrate that the γ-decay of GRs to low-lying vibrational states is an effective approach to access directly the microscopic structure of the GRs. Such kind of analysis can be applied to the study of pygmy resonances about their collectivity and isospin character.

* * *

This research was partly supported by the National Key Research and Development (R&D) Program under Grant No. 2021YFA1601500 and Natural Science Foundation of China under Grant No.12075104.

REFERENCES

[1] Bortignon P. F., Broglia R. A. and Bertsch G. F., *Phys. Lett. B*, **148** (1984) 20.
[2] Ponomarev V. and Krasznahorkay A., *Nucl. Phys. A*, **550** (1992) 150.
[3] Milburn R. H., *Phys. Rev. Lett.*, **10** (1963) 75.
[4] Weller H. R., Ahmed M. W., Gao H., Tornow W., Wu Y. K., Gai M. and Miskimen R., *Prog. Part. Nucl. Phys.*, **62** (2009) 257.
[5] Tanaka K. A., Spohr K. M., Balabanski D. L. *et al.*, *Matter Radiat. Extremes*, **5** (2020) 024402.
[6] Wang H. W., Fan G. T., Liu L. X. *et al.*, *Nucl. Sci. Tech.*, **33** (2022) 87.
[7] von Neumann-Cosel P. and Tamii A., *Eur. Phys. J. A*, **55** (2019) 110.
[8] Bertsch G. F., Bortignon P. F. and Broglia R. A., *Rev. Mod. Phys.*, **55** (1983) 287.
[9] Drozdz S., Nishizaki S., Speth J. and Wambach J., *Phys. Rep.*, **197** (1990) 1.
[10] Shevchenko A., Carter J., Fearick R. W., Förtsch S. V., Fujita H., Fujita Y., Kalmykov Y., Lacroix D., Lawrie J. J., von Neumann-Cosel P., Neveling R., Ponomarev V. Y., Richter A., Sideras-Haddad E., Smit F. D. and Wambach J., *Phys. Rev. Lett.*, **93** (2004) 122501.
[11] Poltoratska I., Fearick R. W., Krumbholz A. M., Litvinova E., Matsubara H., von Neumann-Cosel P., Ponomarev V. Y., Richter A. and Tamii A., *Phys. Rev. C*, **89** (2014) 054322.
[12] Brenna M., Colò G. and Bortignon P. F., *Phys. Rev. C*, **85** (2012) 014305.
[13] Lv W. L., Niu Y. F. and Colò G., *Phys. Rev. C*, **103** (2021) 064321.
[14] Bohr A. and Mottelson B. R., *Nuclear Stucture*, 2nd edition, Vol. **I** (W. A. Benjamin Inc., New York) 1998.
[15] Harakeh M. N. and van der Woude A., *Giant Resonances: Fundamental High-Frequency Modes of Nuclear Excitation* (Oxford University Press, Oxford) 2001.
[16] Bortignon P., Broglia R., Bes D. and Liotta R., *Phys. Rep.*, **30** (1977) 305.
[17] Bohr A. and Mottelson B. R., *Nuclear Stucture*, 2nd edition, Vol. **II** (W. A. Benjamin Inc., New York) 1998.
[18] Colò G., Cao L., Giai] N. V. and Capelli L., *Comput. Phys. Commun.*, **184** (2013) 142.
[19] Cao L. G., Lombardo U., Shen C. W. and Giai N. V., *Phys. Rev. C*, **73** (2006) 014313.
[20] Speth J., Werner E. and Wild W., *Phys. Rep.*, **33** (1977) 127.